Rigid body separation dynamics for space launch vehicles

B. N. Rao
Structural Analysis and Testing Group, Aeronautics Entity
Vikram Sarabhai Space Centre
Trivandrum, India

D. Jeyakumar, K. K. Biswas, S. Swaminathan and E. Janardhana
Launch Vehicle Design Entity
Vikram Sarabhai Space Centre
Trivandrum, India

ABSTRACT

This paper presents a systematic formulation for the simulation of rigid body dynamics, including the short period dynamics, inherent to stage separation and jettisoning parts of a satellite launcher. This also gives a review of various types of separations involved in a launch vehicle. The problem is sufficiently large and complex; the methodology involves iterations at successively lower levels of abstraction. The best choice to tackle such problems is to use state-of-the-art programming technique known as object oriented programming. The necessary classes have been identified to represent various entities in the launch vehicle separation process (e.g., gravity, aerodynamics, propulsion and separation mechanisms etc.). Simple linkages are modelled with suitable objects. This approach helps the designer to simulate a launch vehicle separation dynamics and also to analyse separation system performance. To examine the influence of the design variables on the separating bodies, statistical analyses have been performed on the upper stage separation process and pull out of ongoing stage nozzle from the spent stage of a multistage rocket carrier using retro rockets.

NOMENCLATURE

A_z	launch azimuth (deg)
d_T	distance of thrust location from vehicle longitudinal axis (m)
h	Altitude of separation (km)
I	Inertia tensor (kg-m^2)
l_{CG}	distance of CG from nose tip along longitudinal axis (m)
l_T	distance of thrust location from nose tip along longitudinal axis(m)
m_M, m_S	mass of the ongoing and spent bodies (kg)
m	propellant mass flow rate (kgs^{-1})
R_E, R_P, R_S	Earth's equatorial radius, polar radius, radius at the surface (km)
r, q, p	body angular rates yaw, pitch and roll (deg/s)
$\mathbf{r}_\mathbf{I}$	position vector in ECI frame (X_I, Y_I, Z_I) (m)
$\mathbf{r}_{CG}$	position vector of the body CG offset (m)
r_s	spring location from CG (m)
r_T	distance of thrust location from main body CG (m)
t	time (s)
T	thrust (N)
v	velocity in the body frame (ms^{-1})
X, Y, Z	body axes yaw, pitch and roll
δ	spring mounting azimuth angle (deg)

Paper No. 3007. Manuscript received 1 September 2005, revised 3 January 2006, accepted 24 January 2006.

https://doi.org/10.1017/S0001924000013166 Published online by Cambridge University Press

κ	spring stiffness (N/m)
ξ	stroke length (m)
λ	propulsion unit cant angle (deg)
ρ_D	atmospheric density (kg/m^3)
ρ	azimuth angle of the propulsion unit location measured from *Y*-axis (deg)
ψ,θ,ϕ	yaw, pitch and roll attitude angles wrt LPI frame (deg)
Φ_{GC}	geocentric latitude of the launch station (deg)
Φ_{GD}	geodetic latitude of the launch station (deg)
Θ	launch station longitude (deg)
μ	Earth's gravitational constant (m^3/s^2)
Ω_E	Earth's angular velocity (rad/s)

1.0 INTRODUCTION

The artificial satellite and spacecraft use a multistage rocket as their carrier. Parts of such space vehicle must be separated during flight to jettison stages and components that are no longer needed, to uncover equipment, or to deploy payloads. For a mission to be successful, the separations must occur at the correct times of flight and with minimum changes in the attitude and rotational rates (i.e. tip-off errors of the continuing body). There must be no contact between the separating bodies, no detrimental shock loads induced in the structure, and no excessive or harmful debris. A separation mechanism that does not meet these requirements can produce attitude errors and tumble rates of the continuing body that are too large for its attitude control system to accommodate, can damage its structure and critical equipment, and can cause failure or degradation of the mission. Failure of separation mechanisms has adversely affected mission performance in several instances; for example: The launch failures of Atlas Centaur in 1970 and Chinese Long March in 1992, improper placing of satellite orbits of Titan in 1990, Pegasus in 1991, and Delta-2 in 1995 are some of the typical examples wherein faulty separation systems were suspected to be the main culprits.

1.1 Basic factors in separation mechanisms

In designing separation mechanisms, the following factors must be considered: Adequate clearance between the separating bodies; Shock transmission to the payload or structure of the continuing body; Damage to or contamination of the continuing body by debris and gases from the operation of the separation mechanism; The ability of the mechanism to withstand the natural and induced environments encountered during service.

A separation phase is really more complex: Structural release when thrust is decreasing, specific unsteady aerodynamic phenomena at separation, impact of plume impingement on the structures: thermal, structural and contamination aspects, influence of wind shear or gust during separation itself, separation with 'Champagne cork' effect (for example, impact of stage pull out and separation during the flight of a launch vehicle), coupling with safety sub-systems, software complexity of flight software with respect to the extremely tight scheduling etc. The disengagement between the two bodies in terms of extreme points (with real geometry of the stage including all protuberances), can have contacts; which are particularly difficult to compute taking into account all the physical phenomena that appear during these kinds of phases, as they can modify the geometry during separation. In fact a separation phase can only be approached with the previous thrust decay phase and the following recovery phase after thrust transient, taking into account failure cases, and it is specific to each launcher, at least for the first stages: and overall strategy depends on many more parameters. Payload separation is easier but once again it is most important that no contact has occurred during the separation, which may require COG offset equilibrium and specific manoeuvres to avoid contamination etc. The designer can choose from among a considerable number of separation components that have been designed, tested, and flown on space vehicles. This approach is usually taken to avoid the cost of new designs and tests associated with development of components.

1.2 Staging process

A typical launch vehicle may involve several separation events such as strap-on separation, stage separation, heat shield separation, ullage rocket separation and spacecraft separation (See Fig. 1). In a multistage rocket configuration the most important event is staging. The staging process during the flight of a launch vehicle comprises of a series of events, which takes place in transferring the regime of an ongoing stage to that of the next stage. Obviously, the process commences from the detection of the burn out of the ongoing stage, and continues with the ignition of the next stage and the separation of the spent stage. Ignition of the next stage and the separation of the spent stage may take place concurrently or with a time difference and in any order, depending on vehicle configuration and mission requirements, and they may be programmed before lift off or on the basis of real time in flight monitoring. During the staging process, the orientation control of the vehicle has to be maintained within specified limits – to be defined on consideration of controllability, structural integrity and avoidance of re-contact. Successful staging depends on the proper functioning of the various vehicle systems under the environments and disturbances acting on the vehicle.

1.2.1 Selection of stage separation systems

Stage separation system design and dynamic analysis are the integral parts of the design and development of any multistage launch vehicle. Lower stage separation, especially strap-on separation attracts specific attention if the separation occurs in the dense atmospheric region as the aerodynamics plays a major role in the design of the separation system. The spent stages are discarded from the continuing vehicle as soon as they become redundant in order to minimise the inert weight of the ongoing vehicle. The selected separation system design should ensure collision-free separation between the spent and functional stages and prevent build-up of large lateral velocity to the ongoing functional stages. The spent stages, which are physically separated from the ongoing stage, are pushed away from the vicinity of the functional stage by using jettisoning systems. Flexible linear shaped charge (FLSC) (see Fig. 2) is used to sever the stages and spring thrusters or side rockets are used to provide the required jettisoning velocity, the impulse depending upon the stage inert mass.

In the booster stage separation, an FLSC based severing together with retro-rockets or vented inter stage (VIS) (see Fig. 3) separation systems are used to provide the required separation velocity. In VIS, the continuing stage jet impingement force is used to provide the required jettisoning velocity for the spent body. In heat shield separation, the impulse generated by a zip cord mechanism (see Fig. 4) excites the flexible modes of the heat shield in addition to providing a linear velocity. By superimposing the flexible response over the rigid body motion the dynamic analysis is carried out. The upper stages and spacecraft separation systems use clamp band joints with pyro assisted release mechanisms together with spring thrusters as jettisoning devices. Spring thrusters were used for spacecraft separation due to the requirement of low shock level and contamination free environment. Generally three basic elements are required for the functioning of a separation process: An actuator to trigger the event, usually electric or pyro based; Release/severance system for physical separation; Jettisoning system to impart sufficient relative separation velocity. The severance/release system imparts a physical separation to the bodies; they are primarily of two types: mechanical systems and pyrotechnique devices. The mechanical systems are ball and socket, ball and lock (see Fig. 5), merman band, clamp band, collet (see Fig. 6), cable cutters, pin-pullers etc. The pyrotechnique

https://doi.org/10.1017/S0001924000013166 Published online by Cambridge University Press

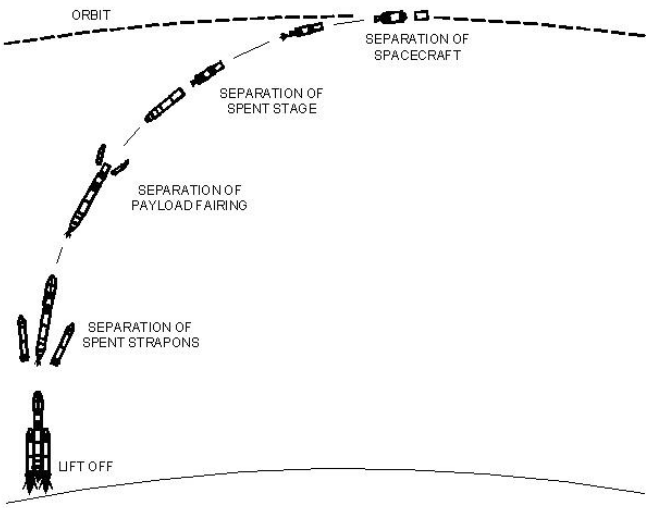


Figure 1. Separation events of a typical launch vehicle.

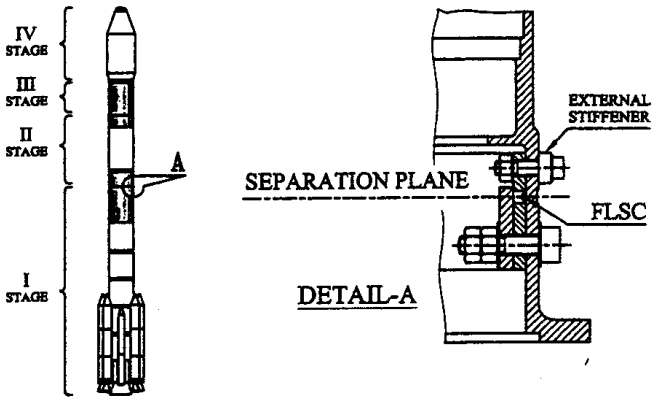


Figure 2. FLSC separation system.

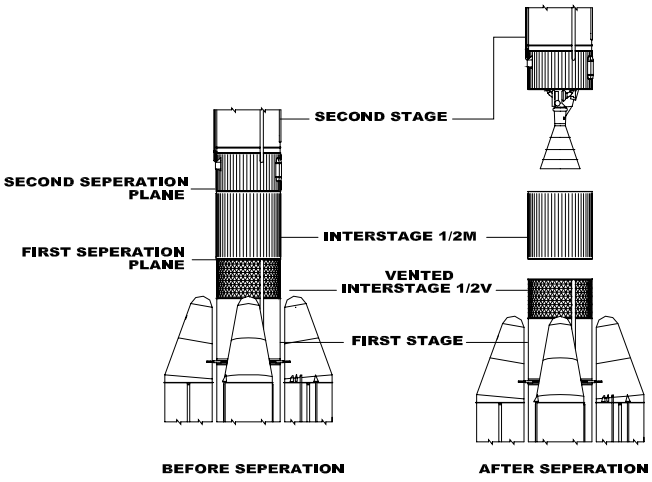


Figure 3. Vented Inter-stage separation System (VIS).

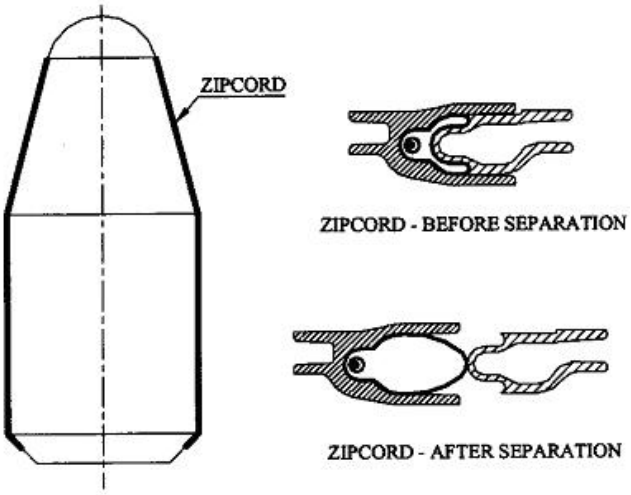


Figure 4. Heat shield separation system using zipcord.

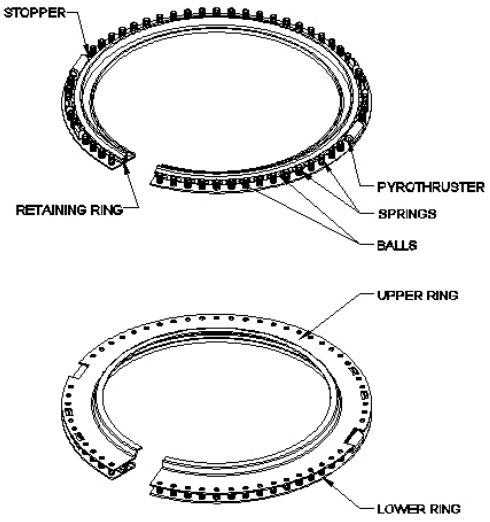


Figure 5. Ball and lock mechanism.

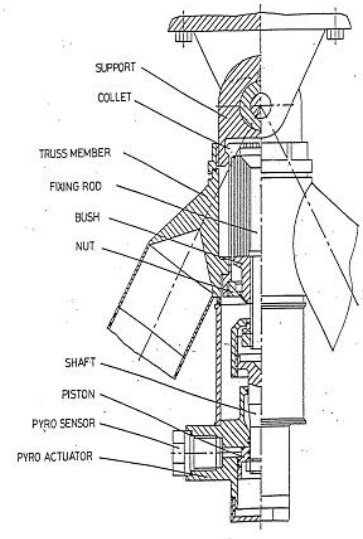


Figure 6. Collet mechanism.

https://doi.org/10.1017/S0001924000013166 Published online by Cambridge University Press

devices are explosive bolts, pyro release nuts, FLSC and also various encapsulated designs like zip and super zip etc.

Separation involves pyro-actuated severance of the designated vehicle elements and imparting of the required relative velocity between the separating bodies through passive or active means. The pyro actuator has to have the capacity with specified minimum margin to do the severance and yet it should not generate shock levels strong enough to damage the modules of the vehicle. The modules located in the vicinity of the severance zone are susceptible to the severance shock. The relative velocity between the separating bodies is generated either by releasing a set of pre-compressed springs or by firing auxiliary rockets. In this activity, angular motion is also unavoidably imparted to the separating bodies.

1.2.2 Stage separations of launch vehicles

In multistage launch vehicles the spent stage separation process is broadly classified into two classes: Separation occurring during atmosphere (booster/lower stage separation); and separation occurring out of atmosphere (vacuum/upper stage) separation. Dynamics of atmospheric separation is very complex due to the presence of aerodynamic forces and moments acting on separating bodies. On the other hand upper stage separations are comparatively simpler due to absence of aerodynamic forces. Lower stage or strap-on separation as the name indicates are the rocket motors strapped on to the core motor to boost the payload capability of the vehicle. These motors are separated from the main vehicle by an on board command once their intended functions are over. The direction of separation can be fixed to avoid collision hazards to the core vehicle, unlike the separations of other stages, which are usually in the axial direction. Separation and jettisoning the strapons is one of the most challenging tasks due to the complexity of separation dynamics analysis involved particularly when the strapons are to be separated in a high dynamic pressure environment and when a number of strap-ons are involved.

For carrying higher payloads, the launch vehicles are often configured to use solid strapon motors. When strapon motors are employed one major concern is the differential thrust between the motors. The differential thrust is highest during the tail off period, which is also the zone of stage separation. This places high demands on control power plant to generate the control force depending upon autopilot signal to stabilise and steer the vehicle, and hence is to be limited. The problem gets complicated when the control power available is also small in non-autonomous control systems like the secondary injection or flex nozzle control systems commonly employed in solid motors. During the separation event, the vehicle control has to pass from the separated stage to the succeeding stage. Where both the stages are solid motors and control is through injection of a fluid into the side of diverging nozzle section ('Secondary injection thrust vector control – SITVC'), some special problems arise, during stage separation. In these cases, control is available only during the motor operation. Even within motor operation, SITVC effectiveness diminishes for motor chamber pressures below a certain value. This situation occurs during the later portion of motor tail-off and during the initial phase of ignition. Hence, if the succeeding stage is not ignited before the pressure drops below a certain value in the earlier stage, loss of vehicle control occurs.

This will result in building up of vehicle orientation errors. This error build-up in the presence of atmospheric dynamic pressure loads on the vehicle could prove detrimental to the vehicle and the mission. A major factor to be considered in designing the separation system and flight sequence is the tail off thrust. Consider the case of separation between two core stages, with lower stage being a solid motor. During the lower stage operation, the vehicle control is obtained by the stage motor action itself (by SITVC or Flex nozzle control). The stage separation should be achieved and the upper stage should take over control without creating large error in orientation. The separation should be carried out before the pressure in the booster solid motor (lower stage) drops to such a low value that its control is not effective. But if separation is done too early, the thrust from the booster stage (tail off thrust) leads to collision between the two separated stages. To ensure collision free separation, retro rockets are incorporated on the separated booster. The sizing of the retro rockets (thrust levels), booster tail off thrust, dynamic pressure on vehicle, vehicle configuration at inter-stage, and separation system force should all be analysed interactively in the separation system design. When the solid motor is followed by a liquid motor there is a requirement of a certain level of positive acceleration before the liquid motor ignition. The ullage motor is provided to ensure this level at separation and is ignited before the thrust from the lower stage solid motor drops below a certain level.

1.2.3 Heat shield separation

The primary function of the heat shield is to protect the payload and other sensitive systems of the launch vehicle from the aerodynamic and thermal loads during the ascent phase of the launch vehicle and to provide the aerodynamic shape thereby reducing the aerodynamic drag. After meeting the functional requirements, the heat shield should be separated from the launch vehicle and from the performance point of view the heat shield has to be separated as early as possible. The system used for separation should impart the necessary jettisoning velocity to achieve collision free separation. The heat shields are usually made in two halves and are attached by the separation system (see Fig. 4). The velocity required for safe separation depends on the heat-shield diameter, mass, and the state of motion at the separation phase (coasting or thrusting) etc. However as the diameter and length of heat shield increase flexibility effects must be considered for safe separation. In most vehicles the heat shields are separated during the thrusting phase. All these factors necessitate a large separation velocity to be provided and the selected jettisoning system has to impart this velocity as quickly as possible. The separation dynamics of the heat shield is generally analysed by combining the rigid body and flexible motions of the fairings using the finite element method.

1.2.4 Essence of rigid body separation dynamics

The separation process is always mission critical, hence the level of the analysis required for an assessment of the adequacy of the separation system is very important. This requires accurate modelling of the various forces and moments on the separating bodies, which are forces and moments due to gravity, retro/ullage rockets, tail off thrust, jet damping, release and jettison mechanisms etc. Information on the critical design parameters can only be obtained from a dynamic study of the separation process. Separation clearances, relative separation velocity requirements, short term and long term collision avoidance, tip-off errors and sensitivity analysis are required from these design support studies. Failure modes and their effects should also be performed wherever possible. If complex forces and moments occur, then six-degree-of-freedom simulations of the separation process are recommended.

1.3 Literature survey

Launch vehicles are almost always multistage using the concept of staging for boosting payload capabilities. This in turn requires jettisoning the spent stages. The dynamics of separating bodies has received the attention of several investigators[1-25]. Chubb[2] has constructed collision boundaries between two separating stages. Dwork[3] and Wilke[4] provide valuable insight into disturbances caused by separation mechanisms in a spin-stabilised set-up.

https://doi.org/10.1017/S0001924000013166 Published online by Cambridge University Press

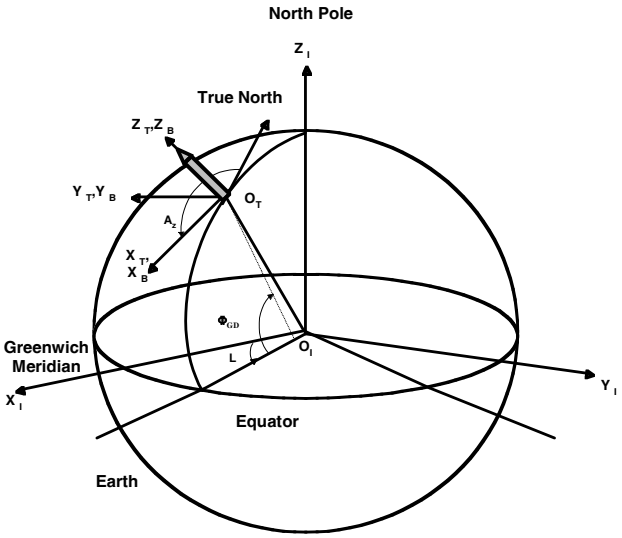


Figure 7. Earth centred inertial (ECI) and launch point inertial (LPI) frames.

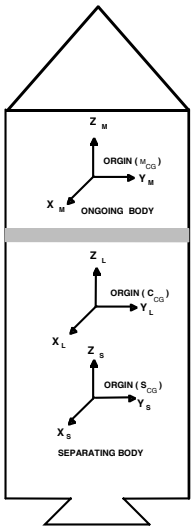


Figure 8. Body and local inertial (CBI) co-ordinate systems.

Considerable aerodynamic data including stability derivatives have been generated for space shuttle type of configurations involving winged bodies[5]. The data so gathered have been utilised for separation dynamics investigation[8]; Waterfall[6] investigated multi-spring system for separation and spinning and non-spinning bodies. Longren[7] analysed spin stabilised rockets with guide shoes and rails constraining the lateral motion. Hurley and Carrie[8] reviewed the genesis of a four bar linkage separation system and carried out the analysis for separation of parallel staged shuttle vehicles. Subramanyam[10] developed a general model for spring assisted stage separation. Biswas[12] investigated several aspects of separation for strap-ons from the launch vehicle. The aerodynamics of separation is complex due to relatively large angles of incidence, intricate geometry, and the involved interference phenomenon. Moraes Jr *et al*[13] developed the Navier-stoke's code, which provided a good agreement with the experiments on the nose part of the ongoing stage. Cheng[14] developed an analytical procedure based on a coupled gas/structure model to simulate the fairing separation events. The procedure was validated by comparing the analysis results with full-scale payload fairing separation test data of Titan IV launch vehicle. Seongjin Choi *et al*[15] developed an efficient three-dimensional aerodynamic-dynamic coupled code to simulate the separation dynamics of strap-on boosters in the dense atmosphere. Lochan *et al*[16-19] analysed the separation dynamics of strap-on boosters from the core rocket utilising the wind tunnel simulation data for dynamic forces and ullage rockets. Jeyakumar and Biswas[20-24] provided stage separation system design and dynamic analysis of ISRO launch vehicles. Jeyakumar, Biswas and Rao[25] examined the stage separation dynamics of the upper stage of a multistage launch vehicle using retro-rockets.

1.4 Objective

This paper presents a systematic formulation for the simulation of rigid body dynamics, including the short period dynamics, inherent to stage separation and jettisoning parts of a satellite launcher. The problem is modelled under the influence of forces and moments of the individual bodies undergoing separation, treating the bodies as rigid. A rigid body has six degrees of freedom (three displacement of a point fixed in the body and three orientation angles). Each body undergoing separation has twelve state variables (namely three displacement of point fixed in the body, three orientation angles, three components of velocity vector and three components of angular velocity vector). Two basic types of frames of reference are used in the formulation apart from the usual geo-centric or earth centreed inertial (ECI) frame of reference (to compute gravity effect) and the topo-centric or launch point inertial (LPI) frame. The first is a local inertial frame (LI-frame) in which the dynamics is described and is essentially the body frame of the combined body rotationally frozen at the instant of separation command but free to travel at a velocity equal to the combined vehicle velocity at separation. This enhances the computation accuracy and makes the results of the analysis easy to comprehend. The second type of frame is the body co-ordinate system (B-frame), separately for each of the body undergoing separation. The transformation from body frame to local inertial frame and *vice versa* can be achieved through a transformation matrix in which a sequence of rotation Euler angles is used.

In principle equations of motion can be expressed in any co-ordinate system. It is advantageous to express them in the body co-ordinate system, as the moments of inertia, engine tail-off thrust and aerodynamic computations are simple in the body co-ordinate system, while gravity computation is simpler in a geo-centric inertial co-ordinate system, transformation from one co-ordinate frame to another is made in the present study as the forces and moments are defined in different co-ordinate systems. The non-linear ordinary differential equations of motion are solved using a fourth-order Runge-Kutta integration scheme. For separation dynamic analysis, it is necessary to simulate the trajectories of the separating bodies taking into account the forces and moments acting on the bodies. To understand the clearances between the separating bodies, critical points will be identified on these bodies. The relative distance between the critical points, relative velocity, body angular velocity and body orientation angles will be estimated for the identification of collision hazards during separation. The trace of the points together with body orientation angles will confirm collision-free clean separation and build up of any tip-off errors on the ongoing functional stage. Graphical simulation of separating bodies will show the occurrence of collision (if any) during separation. For a preliminary dimensioning phase, a fundamental issue addressed in the formulation is the tolerance in the nominal parameters and how they are handled.

https://doi.org/10.1017/S0001924000013166 Published online by Cambridge University Press

2.0 FORMULATION

The physical problem is to simulate the dynamic characteristics of the separating rigid bodies under the influence of disturbing forces and moments. In principle, equations of motion can be expressed in any co-ordinate system. Figures 7 and 8 show the different co-ordinate frames used in the present study. The X_I, Y_I, and Z_I axes as shown in the Fig. 7 define the earth centred inertial (ECI) co-ordinate system. The axes X_I and Y_I lie in the equatorial plane and Z_I is along the North Pole. Gravitational force terms are presented in this co-ordinate system. The X_T, Y_T, and Z_T axes define the Topo-centric or Launch point Inertial (LPI) co-ordinate system. The ECI and LPI coordinates are related through the launch azimuth (A_z), launch site geo-centric latitude (Φ_{GC}) and launch site longitude (Θ). The vehicle orientation at any time is defined with the Euler angles, viz., yaw orientation angle (Ψ), pitch orientation angle (θ), and roll orientation angle (ϕ) with respect to LPI frame. The body frame coincides with LPI frame at the time of launch. It has its origin at the centre of gravity (*CG*) of the individual bodies, namely main (ongoing) body and separating (spent) body as shown in Fig. 8. The X_M, Y_M and Z_M axes with M_{CG} as origin define the main body co-ordinate system. The X_S, Y_S and Z_S axes with S_{CG} as origin define the separating body co-ordinate system. The X_L, Y_L and Z_L axes coincide with body axes of the combined body just before separation. This frame moves with a constant velocity equal to that of the combined body at the instant of separation.

2.1 Equations of motion

The translational and rotational equations of motion for each body in the respective body frame are[20-29] ;

$$m\left\{\frac{d\vec{v}}{dt}\right\}+m\vec{\omega}\times\vec{v}=\vec{F}_{ext} \quad \ldots (1)$$

$$\frac{d\vec{L}}{dt}+\vec{\omega}\times\vec{L}=\vec{M}_{ext} \quad \ldots (2)$$

Here m is the mass of the body; $\vec{v}=v_x\vec{i_b}+v_y\vec{j_b}+v_z\vec{k_b}$, is the velocity; $\vec{\omega}=r\vec{i_b}+q\vec{j_b}+p\vec{k_b}$, is the angular velocity, which has components r, q and p along the body axes, *viz.*, yaw, pitch and roll respectively; t – is time; $\vec{F_{ext}}=F_x\vec{i_b}+F_y\vec{j_b}+F_z\vec{k_b}$, is the total external force vector; $\vec{L}=L_x\vec{i_b}+L_y\vec{j_b}+L_z\vec{k_b}$ is the angular momentum vector; $\vec{M_{ext}}=M_x\vec{i_b}+M_y\vec{j_b}+M_z\vec{k_b}$, is the total external moment vector. $\vec{i_b}$, $\vec{j_b}$, $\vec{k_b}$ are the unit vectors with respect to the centre of mass of the respective body frame.

The components of angular momentum vector are obtained from;

$$\begin{Bmatrix}L_x\\L_y\\L_z\end{Bmatrix}=[I]\begin{Bmatrix}r\\q\\p\end{Bmatrix}=\begin{bmatrix}I_{xx}&I_{xy}&I_{xz}\\I_{yx}&I_{yy}&I_{yz}\\I_{zx}&I_{zy}&I_{zz}\end{bmatrix}\begin{Bmatrix}r\\q\\p\end{Bmatrix} \quad \ldots (3)$$

Here I_{xx}, I_{yy} and I_{zz} are the principal moment of inertia about yaw, pitch and roll (*X, Y, Z*) axes respectively. I_{xy}, I_{xz}, I_{yx}, I_{yz}, I_{zx} and I_{zy} are the products of inertia with respect to the indicated planes, e.g., *xy*, *xz*, *yz*. The symmetry in the products of inertia has been noted. It may be noted that the moments of inertia may only be positive, but the products of inertia may be either positive or negative.

Equation (1) and (2) can be written in the form;

$$\frac{d}{dt}\begin{Bmatrix}v_x\\v_y\\v_z\end{Bmatrix}=\begin{Bmatrix}pv_y-qv_z\\rv_z-pv_x\\qv_x-rv_y\end{Bmatrix}+\frac{1}{m}\begin{Bmatrix}F_x\\F_y\\F_z\end{Bmatrix} \quad \ldots (4)$$

$$\frac{d}{dt}\begin{Bmatrix}r\\q\\p\end{Bmatrix}=[I]^{-1}\begin{Bmatrix}pL_y-qL_z+M_x\\rL_z-pL_x+M_y\\qL_x-rL_y+M_z\end{Bmatrix} \quad \ldots (5)$$

The kinematic differential equations, which provide the relationship between Euler angles and angular velocity components, are

$$\frac{d}{dt}\begin{Bmatrix}\psi\\\theta\\\phi\end{Bmatrix}=\begin{bmatrix}\mathrm{Cos}\phi & -\mathrm{Sin}\phi & 0\\ \dfrac{\mathrm{Sin}\phi}{\mathrm{Cos}\psi} & \dfrac{\mathrm{Cos}\phi}{\mathrm{Cos}\psi} & 0\\ \mathrm{Sin}\phi\dfrac{\mathrm{Sin}\psi}{\mathrm{Cos}\psi} & \mathrm{Cos}\phi\dfrac{\mathrm{Sin}\psi}{\mathrm{Cos}\psi} & 1\end{bmatrix}\begin{bmatrix}r\\q\\p\end{bmatrix} \quad \ldots (6)$$

The motion of bodies in the yaw plane is important in separation dynamics. Hence, the sequence (ψ,θ,ϕ) corresponding to the yaw, pitch, roll is followed in the present study, whereas the sequence for simulation of flight trajectories adopted is (θ,ψ,ϕ). There are singularities in two of the rates of the Euler angles θ and ϕ, which occur in both pitch and roll when $\psi = 90°$. These singularities in Equation (6) are eliminated using L'Hospital's rule[28] and one can obtain expressions that are finite when $\psi = 90°$. In other ways one can resort to Euler four parameters approach and enforce a constraint on the parameters with Lagrange multipliers. For vertically launched vehicles the yaw angles (ψ) will be well below 90°.

Equations (4) to (6) are the governing equations of motion for the individual bodies undergoing separation and are non-linear ordinary differential equations, which are to be solved numerically after specifying the components of total external force and moment vectors. The dynamic characteristics of the separating bodies are modelled here under the influence of the gravity and the spring forces and moments, retro-rocket thrust, jet damping thrust and aerodynamic forces from wind tunnel tests.

2.2 ECI to LPI Transformation

The transformation matrix [T_{EL}], which transfers the components of a vector from ECI frame to LPI frame, is[23,25,27,28];

$$[T_{EL}] = [e_{ij}]_{3\times 3} \quad (7)$$

where;
$e_{11} = -\mathrm{Cos}A_z\mathrm{Sin}\Phi_{GC}\mathrm{Cos}\Theta - \mathrm{Sin}A_z\mathrm{Sin}\Theta$; $e_{12} = -\mathrm{Cos}A_z\mathrm{Sin}\Phi_{GC}\mathrm{Sin}\Theta + \mathrm{Sin}A_z\mathrm{Cos}\Theta$;$e_{13} = \mathrm{Cos}A_z\mathrm{Cos}\Phi_{GC}$;
$e_{21} = -\mathrm{Sin}A_z\mathrm{Sin}\Phi_{GC}\mathrm{Cos}\Theta + \mathrm{Cos}A_z\mathrm{Sin}\Theta$; $e_{22} = -\mathrm{Sin}A_z\mathrm{Sin}\Phi_{GC}\mathrm{Sin}\Theta - \mathrm{Cos}A_z\mathrm{Cos}\Theta$;$e_{23} = \mathrm{Sin}A_z\mathrm{Cos}\Phi_{GC}$;
$e_{31} = \mathrm{Cos}\Phi_{GC}\mathrm{Cos}\Theta$; $e_{32} = \mathrm{Cos}\Phi_{GC}\mathrm{Sin}\Theta$; $e_{33} = \mathrm{Sin}\Phi_{GC}$;

The geocentric latitude of the vehicle position is, $\Phi_{GC} = \mathrm{Sin}^{-1}(Z_1/r_1)$; the geodetic latitude of the vehicle position is, $\Phi_{GD} = \mathrm{Tan}^{-1}\{(R_E/R_P)^2\ \mathrm{Tan}\Phi_{GC}\}$; R_P is the polar radius of the oblate earth geometry; the inertial longitude of the vehicle position is $\Theta_I = \mathrm{Tan}^{-1}(Y_1/X_1)$; the relative longitude with respect to earth is, $\Theta_R = \Theta_I - \Omega_E t$; and the earth rotation rate, $\Omega_E = 7{\cdot}29211 \times 10^{-5}$ rad/s. The altitude of the vehicle in Fig. 9 is: $h = r_I - R_S$; The radius of the earth corresponding to Φ_{GC} is: $R_s = R_E/\sqrt{1+\{(R_E/R_P)^2-1\}\mathrm{Sin}^2\Phi_{GC}}$; the equatorial radius $R_E = 6378{\cdot}1656$km; and the polar radius, $R_P = 6356{\cdot}7838$km.

2.3 LPI to body transformation

The transformation matrix [T_{LB}], which transfers the components of a vector from LPI frame to body frame, is[23,25,27,28]

$$[[T_{LB}] = [b_{ij}]_{3\times 3} \quad (8)$$

where:

$b_{11} = \mathrm{Cos}\phi_0\mathrm{Cos}\theta_0 + \mathrm{Sin}\phi_0\mathrm{Sin}\psi_0\mathrm{Sin}\theta_0$; $b_{12} = \mathrm{Sin}\phi_0\mathrm{Cos}\psi_0$; $b_{13} = -\mathrm{Cos}\phi_0\mathrm{Sin}\theta_0 + \mathrm{Sin}\phi_0\mathrm{Sin}\psi_0\mathrm{Cos}\theta_0$;
$b_{21} = -\mathrm{Sin}\phi_0\mathrm{Cos}\theta_0 + \mathrm{Cos}\phi_0\mathrm{Sin}\psi_0\mathrm{Sin}\theta_0$; $b_{22} = \mathrm{Cos}\phi_0\mathrm{Cos}\psi_0$; $b_{23} = \mathrm{Sin}\phi_0\mathrm{Sin}\theta_0 + \mathrm{Cos}\phi_0\mathrm{sin}\psi_0\mathrm{Cos}\theta_0$;
$b_{31} = \mathrm{Cos}\psi_0\mathrm{Sin}\theta_0$; $b_{32} = -\mathrm{Sin}\psi_0$; $b_{33} = \mathrm{Cos}\psi_0\mathrm{Cos}\theta_0$.

Here ψ_0, θ_0, ϕ_0 are the initial Euler angles. It should be noted that the transformation matrix, T_{LB}, which transfers the components of a

https://doi.org/10.1017/S0001924000013166 Published online by Cambridge University Press

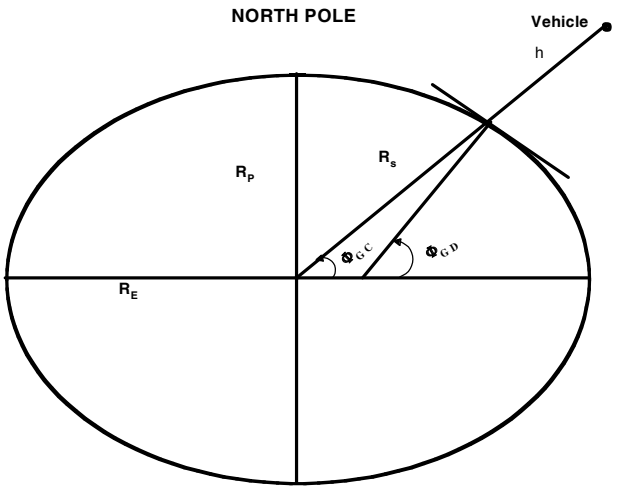


Figure 9. Oblate earth geometry.

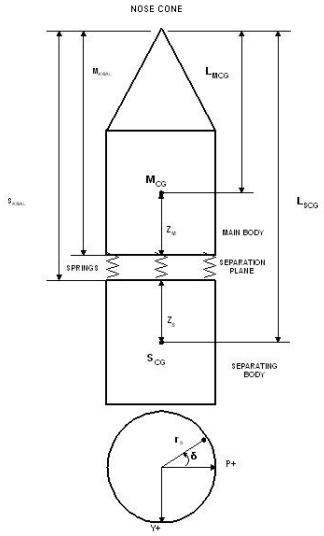


Figure 10. Springs mounted at the separation plane.

vector from the local inertial frame (*LI*) to body frame, is nothing but the transformation matrix T_{LB} has elements as a function of the rotation Euler angles ψ, θ, and ϕ.

2.4 Gravity force and moment computation

The gravitational acceleration along the ECI frame is computed as[28,30];

$$\vec{g}_{EC} = g_{XI}\vec{e}_x + g_{YI}\vec{e}_y + g_{ZI}\vec{e}_z = -grad\,U \quad \ldots (9)$$

where the gravitational potential for the oblate Earth is;

$$U = -\frac{\mu}{r_I}\left[1 - \frac{1}{2}J_2\eta^2\left(3\zeta^2 - 1\right) - \frac{1}{2}J_3\eta^3\left(5\zeta^3 - 3\zeta\right) - \frac{1}{8}J_4\eta^4\left(35\zeta^4 - 30\zeta^2 + 3\right)\right] \quad \ldots (10)$$

$\eta = \frac{R_E}{r_I}; \zeta = \frac{Z_I}{r_I}$; $\vec{r}_I = X_I\vec{e}_x + Y_I\vec{e}_y + Z_I\vec{e}_z$, the vehicle position vector with respect to the ECI frame; $r_I = \sqrt{\vec{r}_I \cdot \vec{r}_I}$ is the radial distance of the vehicle from the earth centre; R_E is the equatorial radius of the oblate earth geometry (see Fig. 9); e_x, e_y, e_z are the unit vectors along the axes of the ECI frame; The gravitational constant, $\mu = 3{\cdot}9860253 \times 10^{14}$ m^3/s^2; Gravitational harmonics $J_2 = 1{\cdot}0827 \times 10^{-3}$; $J_3 = -2{\cdot}3 \times 10^{-6}$; $J_4 = -1{\cdot}8 \times 10^{-6}$. Since g_{EC} the gravitational acceleration (9) is computed in ECI frame, it has to be transformed to the LPI frame. The gravitational acceleration along the body frame, $\vec{g} = g_X\vec{i}_b + g_Y\vec{j}_b + g_Z\vec{k}_b$ computed using the transformation matrices $[T_{EL}]$ and $[T_{LB}]$. The components of the gravity forces in the body frame are:

$$\begin{Bmatrix} g_X \\ g_Y \\ g_Z \end{Bmatrix} = [T_{LB}][T_{EL}] \begin{Bmatrix} g_{XI} \\ g_{YI} \\ g_{ZI} \end{Bmatrix} \quad \ldots (11)$$

The gravity force and moment are computed as;

$$\vec{F}_g = m\vec{g} \quad \ldots (12)$$

$$\vec{M}_g = \vec{r}_{CG} \times \vec{F}_g \quad \ldots (13)$$

where $\vec{r}_{CG} = X_{CG}\vec{i}_b + Y_{CG}\vec{j}_b + Z_{CG}\vec{k}_b$ is the position vector of the vehicle centre of mass. In general, the centre of gravity does not coincide with the centre of mass of the vehicle and the gravitational forces will cause moments about the centre of mass of the vehicle. However, since vehicle dimensions are very small compared to the distance from the Earth centre, the moment due to gravitational forces is small compared to other moments.

2.5 Force and moment due to jettisoning systems

Different types of jettisoning systems are employed to provide the impulse to give a specified relative momentum, and hence separation velocity between separating bodies. However, stage ignition, auxiliary rockets, thrust reversal, and compression springs have been the most frequently used techniques. Stage ignition or 'fire-in-the-hole' staging, where the engine of the continuing stage is ignited at the time of stage separation, eliminates the need for devices to provide the separation impulse, but may require vent openings in the expended stage. Auxiliary rockets that exert either positive thrust on the continuing stage or retro thrust on the expended stage, have been utilised to provide the separation impulse for a variety of boosters. In terms of cost and reliability, springs are ideal separation impulse devices when there are stringent tip-off requirements such as payload separation. Helical compression springs are the most common type of springs used for separation.

2.5.1 Usage of helical compression springs

The separation impulse is provided by release of the energy stored in the helical compression springs. Usually springs are employed for satellite separations due to very low disturbance caused to the sensitive payloads. The forward ends of each spring bear against a centring spring cup on the satellite and, since the springs are laterally stable, no auxiliary guides are used. Spring location and support hardware design is dictated by the geometry requirements. To compensate for undesirable forces and moments in two axes, the present formulation is based on symmetrically located '*n*'– number of springs. Proper calibration, marking, and grouping of springs as pairs has to be followed to minimise tip off errors due to tolerances and possible non-linearity in individual spring characteristics.

The spring mounting location in each body is computed as follows (see Fig. 10). The *Z* component of the spring mounting in each body is given by:

https://doi.org/10.1017/S0001924000013166 Published online by Cambridge University Press

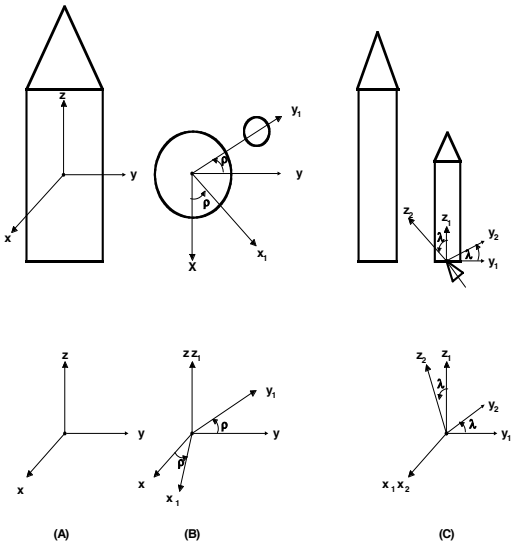


Figure 11. Transformation of retro-rocket thrust frame to body frame.

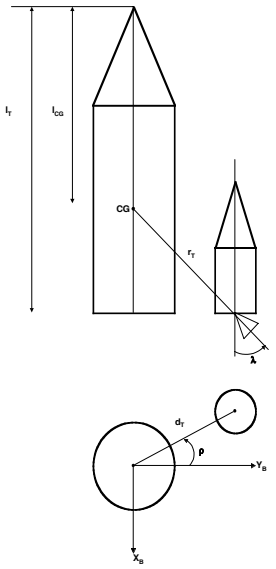


Figure 12. Thrust acting in a retro rocket with respect to main body.

Location of main body *CG* (Z_M) = Location of main body *CG* from nose cone (L_{MCG}) (*m*) – Axial location of spring mounting with respect to main body (M_{AXIAL}) (*m*).

Location of separating body *CG* (Z_S) = Location of separating body *CG* from nose cone (L_{MCG}) (*m*) – Axial location of spring mounting with respect to separating body (S_{AXIAL}) (*m*).

The radial component of spring mounting along *X* and *Y* axes are calculated as $r_S\text{Cos}\delta$ and $-r_S\text{Sin}\delta$, where (r_S) is the radial location (m) of the spring from the *CG* of the individual bodies and δ – is the spring mounting azimuth angle (degrees) measured in anticlockwise direction from P^+ axis. Each of the spring is identified with spring stiffness (that is the force required to compress unit length of the spring), free length, and compressed length. The compressed springs on releasing will generate forces along the springs which generate moments about their respective body *CG*'s. In theory, separation may be effected by a large, single compression spring centrally located, but in practice it is usual to use a large number of smaller springs located symmetrically around the periphery. This is preferred firstly for ease of accommodation and secondly to minimise the possibility of a separation aborting through spring failure. The spring force and moments are given by

$$\overrightarrow{F_S} = \sum_{j=1}^{n} \overrightarrow{F}_{Sj} \qquad \ldots (14)$$

$$\overrightarrow{M_S} = \sum_{j=1}^{n} \left(\overrightarrow{r_{Sj}} \times \overrightarrow{F_{Sj}} \right) \qquad \ldots (15)$$

where $\overrightarrow{r_{Sj}} = X_{Sj}\vec{i} + Y_{Sj}\vec{j} + Z_{Sj}\vec{k}$, is the position vector of the jth spring location; and $\overrightarrow{F}_{Sj} = -\kappa\xi\cos(f_s t)\vec{k}$; κ – is the spring stiffness; and ξ – is the stroke length. The natural frequency of the mass spring system $f_s = 1/2\pi\sqrt{n\kappa/m^*}$, where $m^* = m_M m_s/m_M + m_s$ is the reduced mass. m_M – is the mass of the on going body (satellite) and m_S – is the mass of the separating (spent) body.

2.5.2 Retro-rocket thrust and moment computation

The motion of a spent stage separating from its functional rocket stage by the force of retro thrust is considered. The separation impulse is provided by the relatively low thrust short burn duration solid motor or retro-motors. Its location and support hardware design is dictated by the geometry requirements, as the jet impingement from the retro motor should not affect the highly sensitive payload interface. For each of these thrusts the following information is required. Time measured from initiation of separation *versus* thrust in tabular form. Thrust action point with respect to *CG* of separating body on which thrust is acting. Mounting azimuth angle with respect to vehicle axis. Nozzle exit area, if separation is in the atmosphere. For the thrust given in vacuum the correction is made as follows[29]: Magnitude of actual thrust = Vacuum thrust – (Atmospheric pressure * Nozzle exit area).

To compute the actual thrust from a propulsion unit in the body frame, a transformation matrix is generated between the thrust frame (co-ordinate frame assumed at the nozzle and the body frame is generated as shown in Fig. 11). This matrix is defined by the following sequence of anti clockwise rotation of the body frame: about *Z*-axis through (measured from *Y*-axis) the azimuth angle defining the propulsion unit location; about *X*-axis through λ – nozzle cant angle as shown in Fig. 12.

The thrust vector in the body frame is:

$$\vec{F}_T = T(t)\left(\vec{i}\ \text{Sin}\lambda\ \text{Sin}\rho - \vec{j}\,\text{Sin}\lambda\,\text{Cos}\rho + \vec{k}\,\text{Cos}\lambda\right) \qquad \ldots (16)$$

Propulsion unit thrust location is given by:

$$\vec{r}_T = = d_T(\vec{i}\,\text{Sin}\rho + \vec{j}\,\text{Cos}\rho) + (l_{CG} - l_T)\vec{k} \qquad \ldots (17)$$

Moment due to thrust is given by;

$$\overrightarrow{M}_T = \vec{r}_T \times \vec{F}_T \qquad \ldots (18)$$

2.5.3 Jet damping force and moments

Considering a rotating vehicle having an initial pitch rate (*q*), and with its motor burning, reveals that the mass of gas ejected from the nozzle will have angular momentum. Since the mass is isolated from the vehicle once it leaves the nozzle, it is clear that the total angular momentum of the vehicle itself must decrease. Consequently, angular momentum is no longer conserved within the vehicle and due to this fact alone; the gyroscopic motion of the vehicle is lessened (jet damping effect). The jet damping force and moment are given by[26,29]

https://doi.org/10.1017/S0001924000013166 Published online by Cambridge University Press

$$\vec{F}_J = -\dot{m}\vec{\omega}\times\vec{r}_T \quad \ldots (19)$$

$$\vec{M}_J = \vec{r}_T \times \vec{F}_J \quad \ldots (20)$$

where $-\dot{m}$ is the mass flow rate per unit area (considered a nagative quantity since it decreases the vehicle mass). These jet damping forces and moments are computed in the body co-ordinate system.

2.5.4 Aerodynamic force and moment evaluation

This section is included for completeness but cannot be modelled realistically as explained below. During the flight of strap-on launch vehicles, the strap-on boosters are to be separated in the denser atmosphere. Knowledge of aerodynamic characteristics of separating strapons is essential for the design of the separation mechanisms. The ejection mechanism of the separation system imparts lateral forces on the separating strapons. The aerodynamic forces and moments play critical role in the separation process if it occurs in a region of high aerodynamic pressure. The aerodynamic characteristics of separating strapons are not amenable to theoretical investigations. The flow field around such a configuration is highly complex, being dominated by mutual interference of multiple bodies in close proximity. For such a complicated flow field, wind-tunnel experiments are the prime source of reliable data. The aerodynamic forces and moments act on bodies during its passage through atmosphere[29-32]. These forces and moments are defined with reference to the body axes (see Fig. 13). The components of aerodynamic force and moment are:

$$\begin{Bmatrix} F_{AX} \\ F_{AY} \\ F_{AZ} \end{Bmatrix} = -QS \begin{Bmatrix} C_N \\ C_S \\ C_A \end{Bmatrix} \quad \ldots (21)$$

$$\begin{Bmatrix} M_{AX} \\ M_{AY} \\ M_{AZ} \end{Bmatrix} = \begin{Bmatrix} -F_{AY}\,(l_{CG} - Z_{CY}) \\ F_{AX}\,(l_{CG} - Z_{CP}) \\ QSd\,(C_{RM} + C_{l\delta 1}\delta 1 + C_{l\delta 2}\delta 2) \end{Bmatrix} \quad \ldots (22)$$

where Q is the dynamic pressure (Pa); S is the reference area (m^2); C_N is the normal force coefficient in pitch plane. C_S is the normal force coefficient in yaw plane; C_a is the axial force coefficient. $C_N = C_{N\alpha}\,\alpha$; $C_S = C_{S\beta}\,\beta$; α is the pitch angle of attack and β is the yaw angle of attack in radians. Z_{CP} is centre of pressure location in pitch plane measured from nose tip (m); Z_{CY} is the centre of pressure location in yaw plane measured from nose tip (m); d is the reference diameter (m); C_{RM} rolling moment coefficient with respect to CG of vehicle. $C_{l\delta 1}$ is the rolling moment coefficient due to the strapon motor and SITVC tank; $C_{l\delta 2}$ is the rolling moment coefficient due to fin attachment misalignment. δ_1 is the strapon and SITVC tank mounting misalignment (deg) and δ_2 is the fin mounting misalignment (deg).

The relative velocity of the body with reference to the atmospheric wind and earth rotation is given by:

$$\vec{V}_{RI} = \vec{V}_I - \Omega_E \times \vec{r}_I - \vec{V}_{WI} \quad \ldots (23)$$

where Ω_E – Earth's angular velocity (rad/s); $\vec{r}_I$ is the position vector in ECI frame (m); $\vec{V}_I$ is the inertial velocity components in ECI frame (ms^{-1}); $\vec{V}_{RI}$ is the relative velocity in ECI (ms^{-1}); $\vec{V}_{WI}$ is the wind velocity in ECI (ms^{-1})[33], (see Fig. 14); Mach number M and dynamic pressure Q are defined by:

$$M = \frac{V_{RI}}{V_S}, \quad Q = \frac{1}{2}\rho V_{RI}^{\,2} \quad \ldots (24)$$

The relative velocity $\vec{V}_{RI}$ is transformed to the velocity in body frame

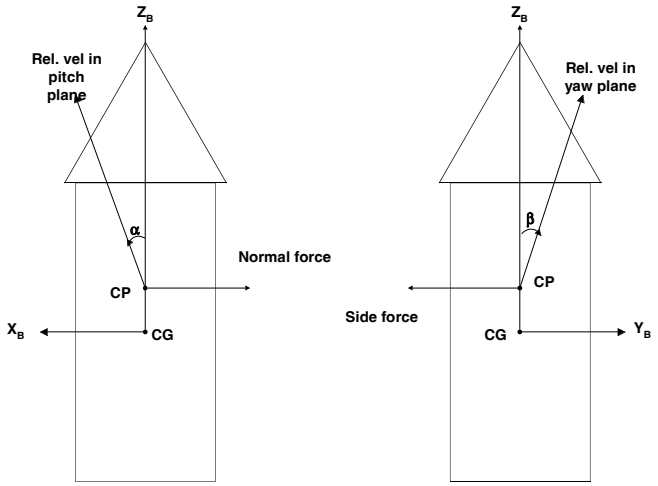


Figure 13. Aerodynamic model.

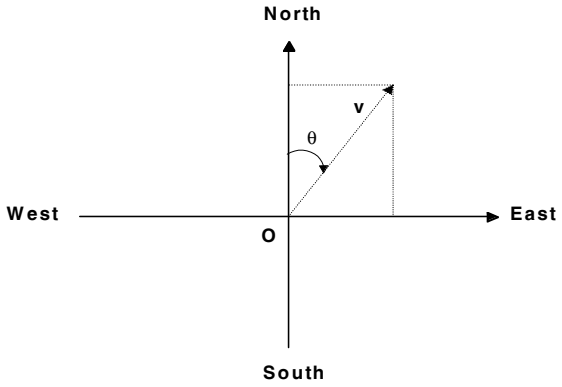


Figure 14. Wind in vector notation.

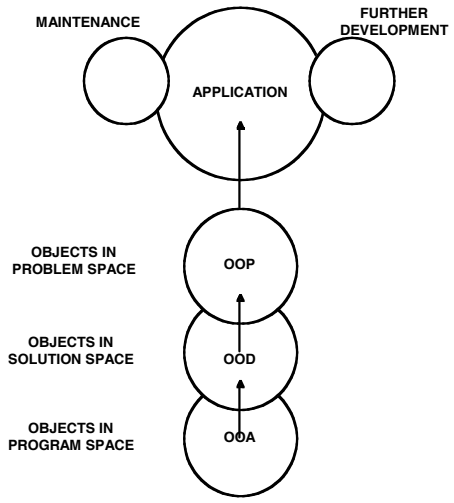


Figure 15. Object oriented software development methodology.

https://doi.org/10.1017/S0001924000013166 Published online by Cambridge University Press

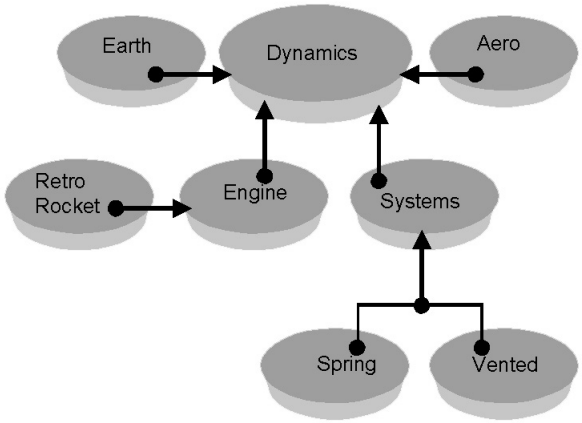


Figure 16. Class architecture.

$\vec{V}_B$ (ms^{-1}). The angle-of-attack is given by;

$$\alpha = \mathrm{Tan}^{-1}\left(\frac{V_{BX}}{V_{BZ}}\right) \textit{ and } \beta = \mathrm{Tan}^{-1}\left(\frac{V_{BY}}{V_{BZ}}\right) \quad \ldots (25)$$

3.0 NUMERICAL SOLUTION

The net external force and moment vectors in equations of motion (1) and (2) are written as;

$$\overrightarrow{F_{ext}} = \overrightarrow{F_g} + \overrightarrow{F_T} + \overrightarrow{F}_S + \overrightarrow{F}_J + \overrightarrow{F}_A \quad \ldots (26)$$

$$\overrightarrow{M_{ext}} = \overrightarrow{M_g} + \overrightarrow{M_T} + \overrightarrow{M_S} + \overrightarrow{M_J} + \overrightarrow{M_A} \quad \ldots (27)$$

With these forces and moments, the solution of equations of motion will give the dynamic characteristics of the individual bodies undergoing separation. Depending on the time in the flight when separation is expected to occur, a rigorous separation analysis considers the respective forces and moments acting on the separating bodies in the equations of motion. A fourth-order Runge-Kutta integration scheme is used to solve the non-linear ordinary differential equations with a fixed time step size of 0·001s. After determining the velocities of the individual bodies at a time '*t*', the relative velocity between the separating bodies in the body frame is calculated.

The magnitude of the body rate is:

$$\left|\vec{\omega}\right| = \sqrt{r^2 + q^2 + p^2} \quad \ldots (28)$$

The relative velocity (v_R) of the separating bodies is:

$$v_R = \sqrt{(v_{x1} - v_{x2})^2 + (v_{y1} - v_{y2})^2 + (v_{z1} - v_{z2})^2} \quad \ldots (29)$$

The relative distance (d_R) from the *CG*'s of the separating bodies is:

$$d_R = \sqrt{(x_1 - x_2)^2 + (y_1 - y_2)^2 + (z_1 - z_2)^2} \quad \ldots (30)$$

Here (v_{x1}, v_{y1}, v_{z1}), (v_{x2}, v_{y2}, v_{z2}), (x_1, y_1, z_1) and (x_2, y_2, z_2) are the components of the velocity vector and position vector of the ongoing and spent body which were transformed to the common body inertial (CBI) frame.

3.1 Identification of collision between separating bodies

For separation dynamic analysis, it is necessary to simulate the trajectories of the separating bodies taking into account of the forces and moments acting on the bodies. To understand the clearances between the separating bodies, critical points will be identified on these bodies. The relative distance between the critical points, relative velocity, body angular velocity and body orientation angles will be estimated for the identification of collision hazards during separation. The trace of the points together with body orientation angles will confirm collision free separation and build up of any tip-off errors on the ongoing functional stage. Graphical simulation of separating bodies will show the occurrence of collision (if any) during separation[34].

After determining the velocities of the individual bodies at a time '*t*', the relative velocity between the separating bodies in the body frame is calculated. Applying the inverse transformation to the relative velocity and integrating with respect to time, the actual separation distance between the bodies is found.

3.2 Object oriented approach

The object-oriented programming (OOP) approach is applied for the development of the separation dynamics simulator for launch vehicles. OOP offers several benefits like data hiding, abstraction, inheritance and polymorphism compared to procedural programming where the emphasis is on doing things rather than the data being used. Data are shared among all the functions participating thereby risking data safety and security. OOP implements programs using classes and objects, data and procedures are given equal importance. Data and functions are encapsulated to ensure data safety and security.

The problem discussed here is sufficiently large and complex that the OOP methodology must be iterated at successively lower levels of abstraction. Objects provide a better modelling of real world parameters. The intention is that the software objects closely mimic objects in the real world maintaining a close correspondence between the external parameters and their software representation. Object Oriented Analysis (OOA) was carried out for identifying objects for the building blocks of the software to be developed. The analysis is basically concerned with the decomposition of a problem into its component parts and establishing a logical model to describe the system functions. Object Oriented Design (OOD) is carried out for the mapping of objects in the problem space into objects in the solution space and creating an overall architectural model[35]. This stage normally uses the bottom up approach (see Fig. 15) to build the structure of the system and the top down functional decomposition approach to design the class member function that provide services.

3.3 Class architecture

Object oriented analysis was carried out to identify the various classes and objects in the present formulation to generate the required forces and moments of the separating bodies. The various classes identified are class earth, class aerodynamics, class engines and class systems. Class spring and class vented are the inherited (derived) class of the parent class 'class systems'. Inheritance is the process whereby one object acquires (gets or receives) characteristics from one or more other objects. Similarly class retro-rocket/ullage rocket is the derived class of the class engines. The class earth provides the necessary information related to gravity, atmosphere and wind. Class aerodynamics contains aerodynamic coefficients of the separating bodies and the member functions.

https://doi.org/10.1017/S0001924000013166 Published online by Cambridge University Press

Class engines deals with thrust-related data at the time of separation. Class architecture thus obtained is shown in Fig. 16 is central to the structure of the program[35]. Appropriate objects were identified in the solution space to establish their relationship.

3.4 Software development

Implementation includes coding and testing. Coding includes writing codes for classes, member functions and the main program that act as driver. Modern versatile programming language C++ is used to design this software through the VC++ developer studio. Fundamental capabilities are provided via C++, the most widely used object oriented programming language. C++ has proved a successful choice as a language for developing an object oriented design environment. The object oriented style of programming allowed the interaction model to be implemented in a direct way. In addition, the exploratory style of programming supported by C++ allowed the program to be rapidly developed and tested. The power of an exploratory environment derives from a structured representation of information and set of integrated tools for manipulating that information. It is a large and complicated environment providing many operations. This complexity is made manageable using the present object oriented approach.

4.0 STATISTICAL ANALYSIS

The design of any engineering system is a process of decision-making, under constraints of uncertainty. The uncertainty in the design process is due to lack of deterministic knowledge of different physical parameters and the uncertainty in the model with which the design is performed. The separation system design process depends on many variable parameters. In reality these parameters occur in statistical sense and hence a statistical approach is more suitable for such problems.

4.1 Monte Carlo simulation

To find sensitivities of the separation system parameters Monte Carlo techniques were used. In this approach, a problem has to be solved many times, each time with a set of deterministic value of the system parameters. These values are selected randomly from the legitimate space of the basic variable, including the approximate knowledge of the probability distribution function of these variables where known. In some simulations success of the system is detected and in other simulations the system fails. The ratio between the numbers of failures to the total number of simulations is used to estimate the probability of the failure of the system. The main disadvantage of Monte Carlo simulation is that large numbers of

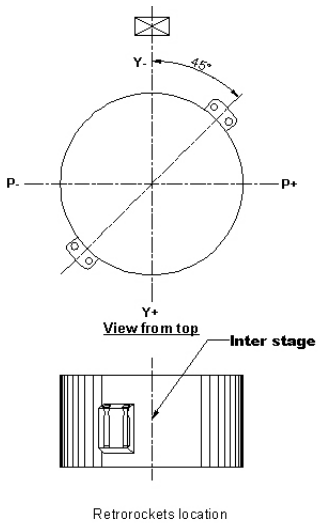


Figure 17. Location of the retro-rockets in a typical launch vehicle.

Table 1
Trajectory parameters at the time of separation

Time of separation '*t*' (s)	300
Altitude of separation '*h*' (km)	140
ECI Position X_I, Y_I, Z_I (m)	460290·075, 6354251·31, 1432314·34
Initial body rate *r*, *q*, *p* (deg/s)	2 for ongoing body and 2·1 for spent body
Initial orientation ψ, θ, ϕ (deg)	0·0, 74·5, 0·0

Table 2
Dynamic parameters of the separating bodies

Parameters	Ongoing body	Spent body
Mass (kg)	34,000 ± 100	12,000 ± 100
Z (mm)	31,000 ± 100	16,000 ± 100
Y (mm)	30 ± 10	50 ± 10
X (mm)	30 ± 10	50 ± 10
I_{ZZ} (kg–m^2)	32,000 ± 10%	50,000 ± 10%
I_{YY} (kg–m^2)	400,000 ± 10%	700,000 ± 10%
I_{XX} (kg–m^2)	400,000 ± 10%	700,000 ± 10%
I_{XY} (kg–m^2)	–50 ± 100%	–150 ± 100%
I_{XZ} (kg–m^2)	–50 ± 100%	–150 ± 100%
I_{YX} (kg–m^2)	–50 ± 100%	–150 ± 100%
I_{YZ} (kg–m^2)	–50 ± 100%	–150 ± 100%
I_{ZY} (kg–m^2)	–50 ± 100%	–150 ± 100%
I_{ZX} (kg–m^2)	–50 ± 100%	–150 ± 100%

Table 3
Comparison of tolerances of the parameters of the separating bodies

Parameters	Worst case method	Monte Carlo simulation		
		–3σ value	Nominal value	+3σ value
Pull out time (s)	1·20	1·212 (1·204)+	1·234 (1·240)	1·256 (1·276)
Relative velocity (m/s)	9·2	8·712 (8·818)	9·084 (9·009)	9·165 (9·199)
Relative longitudinal distance (m)	20·21	20·06 (19·97)	20·21 (20·20)	20·36 (20·42)
Lateral gap available (mm)	579·8	640·8 (646·7)	796·5 (801·4)	935·2 (956·2)
Body rate for ongoing body (°/s)	2·15	2·066 (2·0865)	2·084 (2·0868)	2·102 (2·0872)
Body rate for spent body (°/s)	2·45	1·166 (1·094)	2·232 (2·268)	3·245 (3·441)

+ Predictions based on Multivariate concept

https://doi.org/10.1017/S0001924000013166 Published online by Cambridge University Press

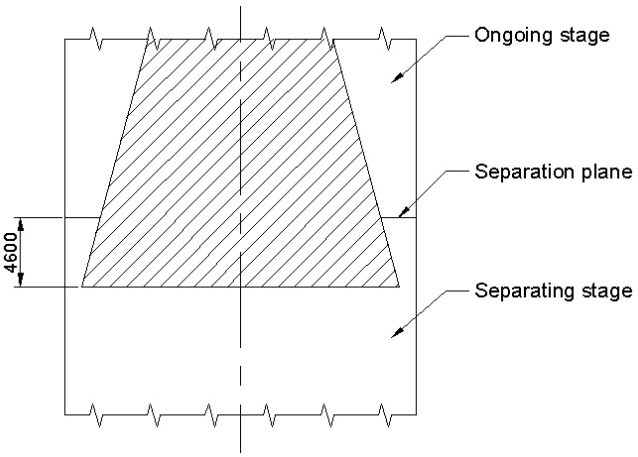


Figure 18. Schematic of the pull out geometry.

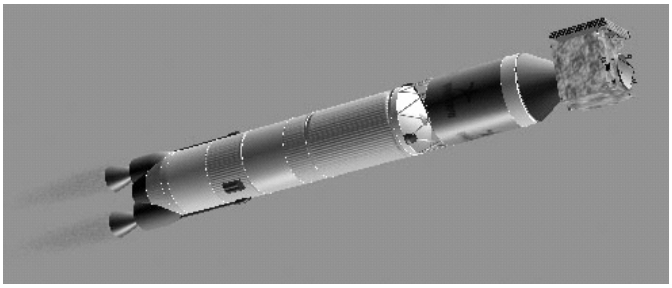


Figure 19. Animation of the stage pull out at the start of separation.

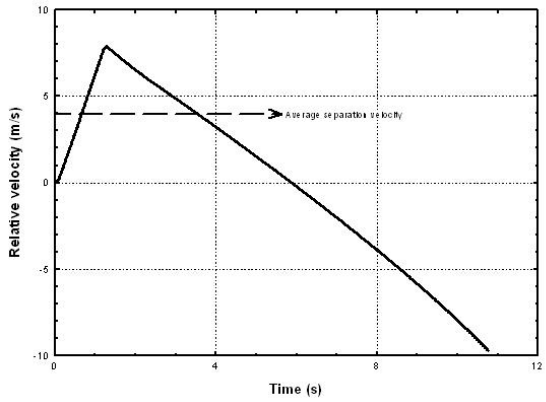


Figure 20(a). Relative velocity of the separating bodies with time.

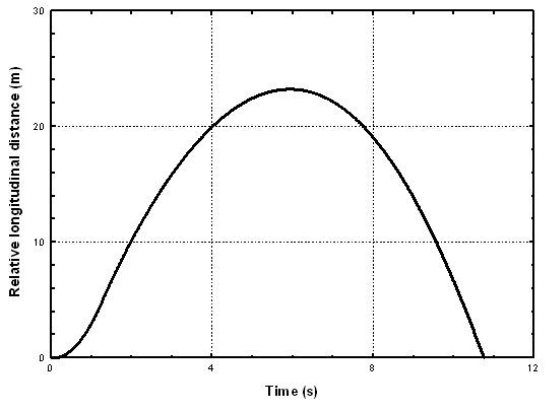


Figure 20(b). Relative longitudinal distance between the separating bodies with time.

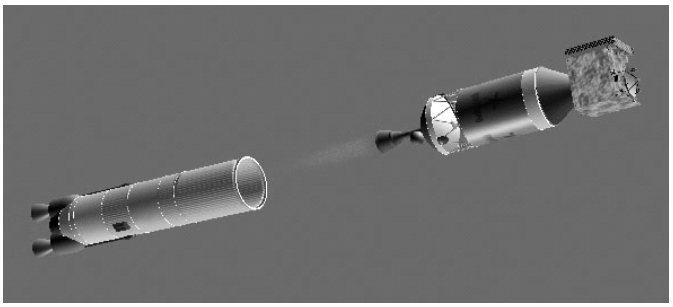


Figure 21. Animation of the stage pull out at the end of separation.

deterministic simulations are required, especially in the tails of the distribution. A very low probability of failures is required in separation dynamics studies (say 10^4 to 10^6 simulations are required for a typical problem). If one simulation run of the problem is in the order of several minutes hence the use of the method becomes prohibitive for practical industrial applications as a result of the large computation time that interferes with the schedule of any project.

4.2 Worst case method

Usual method adopted in separation system design is the worst case studies. In worst case studies, it is assumed that all system parameters have their extreme values in an additive sense and occurrence of collision is predicted. However, a multivariate concept[36], which involves more variable parameters will be more preferable to carry out statistical analysis.

4.3 Multivariate concept

Let the variable function be denoted as Ψ. The variable Ψ be functionally related to 'n' random variables, namely, x_1, x_2...x_n. This function is assumed to be continuous and differentiable. It can be expressed in a Taylor series about a particular point say x_1*, x_2*...x_n*. Neglecting terms of higher order and assuming that the random variables are independent with means at x_1*, x_2*...x_n*, respectively, the expected (average) value of the function is approximately given by;

$$E(\Psi) \approx \Psi(x_1^*, x_2^*, x_3^* \ldots\ldots, x_n^*) + \frac{1}{2}\sum_{i=1}^{n} Var(x_i)\frac{\partial^2 \Psi}{\partial x_i^2} \qquad \ldots (31)$$

And the variance of the function, is approximately given by;

$$Var(\Psi) \approx \sum_{i=1}^{n} Var(x_i)\left(\frac{\partial \Psi}{\partial x_i}\right)^2 \qquad \ldots (32)$$

The partial derivatives of in Equations (31 and 32) are taken at the point x_1*, x_2*...x_n*, and thus are constants. Further more, if the x_i's are normally distributed, Ψ is approximately normally distributed[36].

If the tolerances of the individual variables all fall with in their specification limit, then the tolerances for the function, with 99·9% confidence level will not exceed $E(\Psi) \pm 3\sqrt{\mathbf{var}(\Psi)}$. The square root of the variance of a quantity is the standard deviation of that quantity.

4.3 Evaluation of expected physical quantities

In the present study there are 12 variable functions namely velocity components (v_x,v_y,v_z), position components (x,y,z), angular velocity (r,q,p), body orientation components (ψ,θ,ϕ). These variable functions are related to the dynamic parameters of the separating bodies like mass, moment of inertia, *CG* offset and separation rocket parameters like cant angle, thrust, ignition delay etc. For the variations

https://doi.org/10.1017/S0001924000013166 Published online by Cambridge University Press

in the specified dynamic parameters, the above-described statistical analysis will be useful to find the expected value and variance of the twelve variable functions for the ongoing and spent body. With these values, the body rate for ongoing and spent body, relative velocity and relative distance between the separating bodies can be estimated. Finally it is possible to estimate the tolerances of the physical quantities.

For the present problem the random variables x_1, $x_2 \ldots x_n$. are considered as the specified dynamic parameters. In general the variable functions Ψ_i's (i = 1 to 12) correspond to velocity components (v_x, v_y, v_z), position components (x,y,z), angular velocity components (r,q,p), and the body orientation angles (ψ,θ,ϕ). The values of Ψ_i's are obtained for the average values of dynamic parameters. To find the values of first and second derivatives of Ψ_i's with respect to the dynamic parameters the following procedure is adopted.

For each variable function Ψ_i, the functional values generated by specifying a value of dynamic parameter close to its average and the rest of the dynamic parameters are specified by their average values. The generated data is fitted in to a cubic polynomial of the varied dynamic parameter. The first and second derivative of the function with respect to that dynamic parameter is found out from the cubic polynomial at its average value. This procedure is repeated for all the variable functions and dynamic parameters to obtain the first and second derivatives of variable functions with respect to each dynamic parameter at its average value. Considering variances in the dynamic parameters and the first and second derivatives of variable functions with respect to those dynamic parameters (Equations (31 and 32)) give the expected value of the function and its variance.

5.0 CASE STUDY

To examine the influence of the design variables on the separating bodies, statistical analyses have been performed on the lateral and longitudinal dynamics associated with separation and pull out of an ongoing functional stage from the spent stage of a multistage launch vehicle using retro-rockets as jettisoning systems. Figure 17 shows the location of retro-rockets (separation motors) placed in pairs diametrically opposite. Figure 18 shows the schematic of the actual pull out length. Tables 1 and 2 give the trajectory and dynamic parameters for the separating bodies at the time of separation. Figure 19 shows the combined vehicle at the start of separation. Table-3 gives comparison of tolerances of the parameters of the separating bodies. As per the Monte Carlo simulation the expected pull out time is 1·234s and its tolerance is from 1·212s to 1·256s. The worst-case method gives the pull out time as 1·2s. The initial longitudinal distance just before pull out between the *CG* of the separating bodies is 15·56m. The expected longitudinal distance between the *CG* of the individual body at the separation time is 20·2m. The actual pull out completed at the specified separation time is 4·64m. For the specified nominal design parameters, Fig. 20 shows the variation of the relative velocity and relative longitudinal distance between the separated bodies with separation time. The relative velocity gradually increases up to 8ms^{-1} due to retro action. The relative longitudinal distance increases with separation time up to six seconds due to retro action and decreases with time due to the spent stage tail off thrust (~10kN). To avoid collision between the separating bodies, the ongoing functional stage should be ignited before 10·8 seconds as it is seen from Fig. 20(b). However, a longitudinal gap of 10m between the separating bodies can avoid nozzle damage (ongoing) due to reflected jet plume from the spent body. The stage sequencing should be made accordingly. Figure 21 shows the animation of the stage pull out at the end of separation. The nozzle end diameter is 1·6m. The spent body diameter is 4m. The lateral clearance available (excluding the attachments) for the pull out is 1m. The lateral gap consumed during the nozzle pull out of 4·6m is 204mm due to variations in the dynamic parameters of the separating bodies and the jettisoning systems. As per the Monte Carlo simulation, the minimum lateral gap available between the nozzle end and the burn out body is 641mm, whereas the worst case method gives the result as 580mm. Hence collision free separation of bodies can be expected. It should be noted that +3σ values of the relative velocity and body rates for ongoing and spent bodies are comparable with the worst-case analysis. The –3σ values of the pull out time and available lateral gap are comparable with the worst-case analysis. In general, Monte Carlo simulation as well as worst-case method consume enormous amount of computational time compared to the procedure based on the multivariate concept. Worst-case method gives conservative estimates.

6.0 CONCLUSIONS

A systematic formulation is provided for the simulation of rigid body dynamics useful for the analysis of stage separation and jettisoning parts of a satellite launch vehicle. Specifying the respective forces and moments acting on the separating bodies in equations of motion, the relative velocity, relative position, attitude and attitude rates of the separating bodies can be found for confirmation of the collision-free separation. For a preliminary dimensioning phase, a fundamental pre-requisite is the formulation of the tolerance in the nominal parameters and how they are handled are also addressed. Future articles will be focused on strapon separation, stage pull out and separation and satellite separation for a typical launch mission.

ACKNOWLEDGEMENT

The authors wish to acknowledge the reviewers of VSSC Editorial Board for their valuable suggestions/comments to improve the clarity of the paper. They are thankful to Director, VSSC for clearing the paper for publication.

REFERENCES

1. WASKO, R.A. Experimental investigation of stage separation aerodynamics, NASA-TND-868, 1961.
2. CHUBB, W. The collision boundary between the two separating stages of the SA-4 Saturn Vehicle, NASA-TND-598, 1961.
3. DWORK, M. Coning effects caused by separation of spin stabilized stages, *AIAA J*, 1963, **1**, (11), pp 2639-2640.
4. WILKE, R.O. Comments on coning effects caused by separation of spin stabilized stages, *AIAA J*, 1964, **2**, (7), p 1358.
5. DECKER, J.P. and GERA, J. An exploratory study of parallel – stage separation of reusable launch vehicles, NASA-TND-4765, 1968.
6. WATERFALL, A.P. A Theoretical study of the multi-spring stage separation system of the Black Arrow satellite launcher, RAE-TR-682016, 1968, Farnborough, Hants, UK.
7. LONGREN, D.R. Stage separation dynamics of spin stabilized rockets, *J Spacecraft and Rockets*, 1970, **7**, pp 434-439.
8. HURLEY Jr, M.J. and Carrie, G.W. Stage separation of parallel-staged shuttle vehicles: A capability assessment, *J Spacecraft and Rockets*, 1972, **9**, pp 764-771.
9. ORLIK RUKEMANN, K.J. and IYENGAR, S. Example of dynamic interference effects between two oscillating vehicles, *J Spacecraft and Rockets*, 1973, **10**, pp 617-619.
10. SUBRAMANYAM, J.D.A. Separation dynamics analysis for a multistage rocket, Proceedings of the International Symposium of Space Science and Technology, 1973, pp 383-390, AGNE Publishing, Tokyo, Japan.
11. DECKER, J.P. and WILHITE, A.W. Technology and methodology of separating two similar size aerospace vehicles within the atmosphere, AIAA paper 75-29, 1975.
12. BISWAS, K.K. Some aspects of jettisoning dynamics related to launch vehicles, *Space Dynamics & Celestial Mechanics*, 1986, pp 369-379, Holland.
13. MORAES JR, P., ZDRAVISTCH, F. and AZEVEDO, J.L.F. Aerodynamics of the Brazilian satellite launch vehicle (VLS) during first stage separation, AIAA paper 90-3098, 1990.

https://doi.org/10.1017/S0001924000013166 Published online by Cambridge University Press

14. CHENG, S.C. Payload fairing separation dynamics, *J Spacecraft and Rockets*, 1999, **36**, pp 511-515.
15. SEONGJIN CHOI, CHONGAM KIM, OH-HYUN RHO and JEONG-JOO PARK, Numerical analysis on separation dynamics of strap-on boosters in the atmosphere, *J Spacecraft and Rockets*, 2002, **39**, pp 439-446.
16. RAJEEV LOCHAN, ADIMURTHY, V. and KUMAR, K. Separation dynamics of strap-on boosters, *J Guidance*, *Control and Dynamic*s, 1992, **15**, (1), pp 137-143.
17. RAJEEV LOCHAN, Dynamics of bodies separating from launch vehicles, Ph.D. Dissertation, 1993, Department of Aerospace Engineering, Indian Institute of Technology, Kanpur, India.
18. RAJEEV LOCHAN, ADIMURTHY, V. and KUMAR, K. Separation dynamics of ullage rockets, *J Guidance*, *Control and Dynamics*, 1994, **17**, (3), pp 426-434.
19. RAJEEV LOCHAN and ADIMURTHY, V. Separation dynamics of strap-on boosters in the atmosphere, *J Guidance*, *Control and Dynamics*, 1997, **20**, (4), pp 633-639.
20. JEYAKUMAR, D. and BISWAS, K.K. Stage separation system design and dynamic analysis of ISRO launch vehicles, *J Aerospace Sciences and Technologies*, 2003, **55**, pp 211-222.
21. JEYAKUMAR, D. and BISWAS, K.K. Design and analysis of the stage separation system of a massive liquid rocket stage, Proceedings of the International Conference on Modelling Simulation and Optimisation for Design of Multidisciplinary Engineering Systems, 2003, Goa, India.
22. JEYAKUMAR, D. and BISWAS, K.K. SPECTRA: Separation dynamic simulator for launch vehicles, an object oriented approach , Proceedings of the Twenty-fifth National Systems Conference (On systems engineering approach to sustained growth), 2001, pp 26-34, Allied Publishers Limited, New Delhi, India.
23. JEYAKUMAR, D. and BISWAS, K.K. Multibody dynamic simulator for launch vehicles stage separation studies, Proceedings of the 54th International Astronautical Congress of the International Astronautical Federation, the International Academy of Astronautics, and the International Institute of Space Law, IAC-03-A.6.08, 2003, Bremen, Germany.
24. BISWAS, K.K. and JEYAKUMAR, D. Upper stage separation system studies of launch vehicles using statistical approach, Proceedings of the National Seminar on Aerospace Related Mechanisms (ARMS-96): Modelling and Simulations, 1996, pp 22-28, Vikram Sarabhai Space Centre, Trivandrum, India.
25. JEYAKUMAR, D., BISWAS, K.K. and NAGESWARA RAO, B. Stage separation dynamic analysis of upper stage of a multistage launch vehicle using retro rockets, *J Mathematical and Computer Modelling*, 2005, **41**, (8/9), pp 849-866.
26. BALL, K.J. and OSBORN, G.F. *Space Vehicle Dynamics*, 1967, pp 59-61, Oxford University Press.
27. THOMSON, W.T. *Introduction to Space Dynamics*, 1961, Wiley, New York, USA.
28. REGAN, F. J. *Re-Entry Vehicle Dynamics*, AIAA Education Series, 1984, AIAA, New York, USA.
29. CORNELISSE, J.W., SCHOYER, H.F.R. and WAKKER, K.F. *Rocket Propulsion and Space flight Dynamics*, 1979, Pitman Publishing Limited, London, UK.
30. BRAUER, G. L., CORNICK, D.E., HABEGER, A.R., PETERSEN, F.M. and STEVENSON, R. Program to optimise simulated trajectories (POST), NASA-CR-132689, 1975.
31. THEODORE, T. Introduction to the aerodynamics of flight, NASA SP-367, 1975, Langley Research Center.
32. ANDERSON, J. D. *Fundamentals of Aerodynamics*, 1991, McGraw-Hill, New York, USA.
33. GEISSLER, E.D. *Wind Effects on Launch Vehicles*, 1970, Techinivision services, England, UK.
34. NASA Space Vehicle Design Criteria (Structues), Flight Separation Mechanisms, NASA SP-8056, 1970.
35. BALAGURUSAMY, E. *Object Oriented Programming with C++*, 1995, Tata McGraw, Hill Publishing Company Ltd, New Delhi, India.
36. BOWKER, A.H. and LIEBERMAN, G.I. ENGINEERING STATISTICS, 1972, Prentice Hall, Englewood, Cliffs, NJ, USA.

https://doi.org/10.1017/S0001924000013166 Published online by Cambridge University Press